Binding of Pro-Gly-Pro at the active site of leukotriene A_4 hydrolase/aminopeptidase and development of an epoxide hydrolase selective inhibitor

Alena Stsiapanava[a], Ulrika Olsson[a,1], Min Wan[a,1], Thea Kleinschmidt[a,1], Dorothea Rutishauser[b], Roman A. Zubarev[b], Bengt Samuelsson[a,2], Agnes Rinaldo-Matthis[a], and Jesper Z. Haeggström[a,2]

Divisions of [a]Physiological Chemistry II and [b]Physiological Chemistry I, Department of Medical Biochemistry and Biophysics, Karolinska Institutet, S-171 77 Stockholm, Sweden

Contributed by Bengt Samuelsson, February 4, 2014 (sent for review January 9, 2014)

Leukotriene (LT) A_4 hydrolase/aminopeptidase (LTA4H) is a bifunctional zinc metalloenzyme that catalyzes the committed step in the formation of the proinflammatory mediator LTB_4. Recently, the chemotactic tripeptide Pro-Gly-Pro was identified as an endogenous aminopeptidase substrate for LTA_4 hydrolase. Here, we determined the crystal structure of LTA_4 hydrolase in complex with a Pro-Gly-Pro analog at 1.72 Å. From the structure, which includes the catalytic water, and mass spectrometric analysis of enzymatic hydrolysis products of Pro-Gly-Pro, it could be inferred that LTA_4 hydrolase cleaves at the N terminus of the palindromic tripeptide. Furthermore, we designed a small molecule, 4-(4-benzylphenyl) thiazol-2-amine, denoted ARM1, that inhibits LTB_4 synthesis in human neutrophils (IC_{50} of ∼0.5 μM) and conversion of LTA_4 into LTB_4 by purified LTA4H with a K_i of 2.3 μM. In contrast, 50- to 100-fold higher concentrations of ARM1 did not significantly affect hydrolysis of Pro-Gly-Pro. A 1.62-Å crystal structure of LTA_4 hydrolase in a dual complex with ARM1 and the Pro-Gly-Pro analog revealed that ARM1 binds in the hydrophobic pocket that accommodates the ω-end of LTA_4, distant from the aminopeptidase active site, thus providing a molecular basis for its inhibitory profile. Hence, ARM1 selectively blocks conversion of LTA_4 into LTB_4, although sparing the enzyme's anti-inflammatory aminopeptidase activity (i.e., degradation and inactivation of Pro-Gly-Pro). ARM1 represents a new class of LTA_4 hydrolase inhibitor that holds promise for improved anti-inflammatory properties.

inflammation | leukotriene B_4 | drug development | X-ray crystallography | enzyme mechanism

Leukotriene (LT) A_4 hydrolase/aminopeptidase (EC 3.3.2.6) is a bifunctional zinc metalloenzyme that catalyzes the formation of the potent chemotactic agent LTB_4, a key lipid mediator in the innate immune response (1, 2). Previous work has shown that LTA_4 hydrolase (LTA4H) is an aminopeptidase with high affinity for N-terminal arginines of various synthetic tripeptides (3, 4). The two enzyme activities of LTA4H are exerted via distinct but overlapping active sites and depend on the catalytic zinc, bound within the signature HEXXH-$(X)_{18}$-E, typical of M1 metallopeptidases (5–7). In LTA4H, His295, His299, and Glu318 are the zinc-binding ligands, whereas Glu296 is the general base catalyst for peptide hydrolysis (8, 9).

LTA4H's crystal structure has been determined (10). The enzyme folds into an N-terminal domain, a catalytic domain, and a C-terminal domain, each with ∼200 amino acids. The interface of the domains forms a cavity, where the active site is located (Fig. 1). The cavity narrows at the zinc-binding site, forming a tunnel into the catalytic domain. The opening and wider parts of the cavity are highly polar; the tunnel is more hydrophobic. The cavity is mostly defined by the catalytic and C-terminal domains; part of the tunnel is defined by the N-terminal domain. Bound substrate is in contact with all three domains.

Recently, it was discovered that LTA4H cleaves and inactivates the chemotactic tripeptide Pro-Gly-Pro, thus identifying a previously unrecognized endogenous, physiologically significant aminopeptidase substrate (11). Inasmuch as Pro-Gly-Pro attracts neutrophils and promotes inflammation, these data also suggest that LTA4H plays dual and opposite roles during an inflammatory response (i.e., production of chemotactic LTB_4, as well as inactivation of chemotactic Pro-Gly-Pro). Previous efforts to develop inhibitors of LTA4H have used the aminopeptidase activity for screening purposes, and these molecules therefore block both catalytic activities of LTA4H (12).

Here, we used crystallography, MS, and a stable peptide analog to determine the binding mode of Pro-Gly-Pro at the active site of LTA4H, as well as the mechanism of peptide cleavage. Based on the structure, we also designed a lead compound that selectively blocks the conversion of LTA_4 into LTB_4, although sparing the hydrolysis of Pro-Gly-Pro.

Results and Discussion

Binding of Pro-Gly-Pro at the Active Site of LTA4H. To understand how LTA4H recognizes and cleaves Pro-Gly-Pro, we determined its binding site and conformation by X-ray crystallography. Initially, we tried to determine the structure of an inactive LTA4H mutant (i.e., E296Q), in complex with Pro-Gly-Pro. After several

Significance

Leukotriene (LT) A_4 hydrolase/aminopeptidase (LTA4H) is a bifunctional zinc metalloenzyme that catalyzes biosynthesis of the proinflammatory mediator, LTB_4, implicated in chronic inflammatory diseases. Recently, the chemotactic tripeptide Pro-Gly-Pro was identified as the enzyme's endogenous peptidase substrate. Pro-Gly-Pro is cleaved and inactivated by LTA4H, suggesting that LTA4H plays a role in both the initiation and the resolution phase of inflammation. Here, we defined the binding and cleavage mechanism for Pro-Gly-Pro at the active site of LTA4H. Moreover, we designed a small molecule that selectively blocks synthesis of LTB_4, although sparing the peptidase activity for inactivation of Pro-Gly-Pro, thus representing a novel type of LTA4H inhibitor that may pave the way for development of better treatments of inflammatory diseases.

Author contributions: A.S., U.O., R.A.Z., B.S., A.R.-M., and J.Z.H. designed research; A.S., M.W., T.K., and D.R. performed research; U.O. and A.R.-M. contributed new reagents/analytic tools; A.S., U.O., M.W., T.K., D.R., R.A.Z., B.S., A.R.-M., and J.Z.H. analyzed data; and A.S. and J.Z.H. wrote the paper.

The authors declare no conflict of interest.

Freely available online through the PNAS open access option.

Data deposition: The atomic coordinates and structure factors have been deposited in the Protein Data Bank, www.pdb.org (PDB ID codes 4MS6, 4L2L, and 4MKT).

[1]U.O., M.W., and T.K. contributed equally to this work.

[2]To whom correspondence may be addressed. E-mail: bengt.samuelsson@ki.se or jesper.haeggstrom@ki.se.

This article contains supporting information online at www.pnas.org/lookup/suppl/doi:10.1073/pnas.1402136111/-/DCSupplemental.

Fig. 1. Position and extension of the active center in LTA4H. Cartoon representation of the structure of LTA4H with a tunnel for LTA_4 (red mesh) and peptide substrates (blue mesh). The catalytic zinc (yellow sphere) is located in a wide section of the active site from which a narrow, L-shaped, hydrophobic tunnel protrudes ~15 Å deeper into the protein. LTA_4 is believed to bind with its ω-end at the end of the hydrophobic tunnel. The volume of the active center was calculated in CAVER (31).

attempts with high-resolution data, the X-ray analysis yielded ambiguities in the electron density for the tripeptide, making it difficult to determine details of its binding conformation. Although incomplete, the X-ray data indicated that Pro-Gly-Pro was bound with its C terminus coordinating the catalytic zinc, which, in turn, suggested that LTA4H may act as a carboxypeptidase against the tripeptide (Fig. S1). Instead of using an inactive mutant, we set out to analyze the binding mode of Pro-Gly-Pro using WT LTA4H. To allow use of WT LTA4H, we synthesized a minimally altered analog of Pro-Gly-Pro [i.e., *N*-(4-oxo-4-pyrrolidinyl-butanoyl)-proline], denoted OPB-Pro, in which the original glycyl nitrogen has been exchanged for a carbon, thus preventing N-terminal peptide cleavage (Fig. 2). OPB-Pro was cocrystallized with LTA4H, and we could determine a complex structure to a resolution of 1.72 Å (Fig. 2). OPB-Pro was bound to the enzyme, with its aminoterminus coordinating the zinc ion in a manner compatible with peptide cleavage from this end of the substrate (4).

LTA4H Cleaves Pro-Gly-Pro from Its N Terminus. The structure of Pro-Gly-Pro in complex with the mutant E296Q indicated that LTA4H may act as a carboxypeptidase against the tripeptide

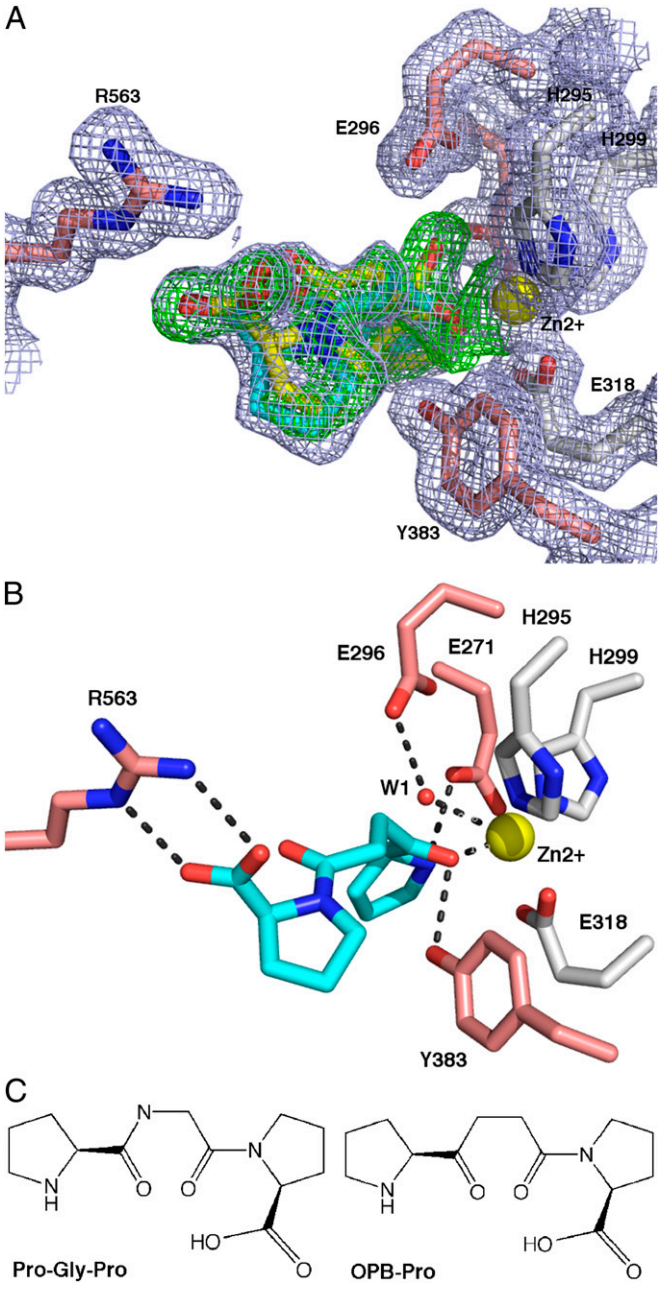

Fig. 2. Crystal structure of the active site of LTA4H in complex with the substrate analog OPB-Pro. (*A*) Active site residues and OPB-Pro are shown in stick representation. The $2mF_o - DF_c$ electron density map is shown as gray mesh (contoured at 1 σ), and the omit map ($mF_o - DF_c$ calculated omitting OPB-Pro and water molecules) is shown as green mesh (contoured at 3 σ). The zinc-binding residues are colored gray, the residues of peptidase active site are colored pink, the yellow sphere represents the zinc ion, and the red spheres represent the oxygen atom of the water molecule. OPB-Pro is presented in two alternative binding modes (shown in cyan and yellow). (*B*) OPB-Pro–binding interactions in the A configuration (details are provided in main text). (*C*) Comparison of the chemical structures of Pro-Gly-Pro and the analog OPB-Pro.

(Fig. S1), whereas the structure of the WT enzyme in complex with OPB-Pro suggested an aminopeptidase reaction (Fig. 2). To determine unambiguously the mechanism by which LTA4H hydrolyses Pro-Gly-Pro, we analyzed the degradation products by high-resolution MS. The primary spectrum contained a major ion at *m/z* 173.1, which could originate from both Gly-Pro and Pro-Gly, the two products of aminopeptidase and carboxypeptidase activity, respectively (Fig. 3). Upon fragmentation of the product mass at *m/z* 173.1, a single major peak appeared at *m/z* 116.2 (Fig. 3), corresponding to the characteristic y1-ion of the dipeptide Gly-Pro. Fragment ions of Gly-Pro are listed in Table S1. We also analyzed degradation products obtained in the presence of $H_2{}^{18}O$ and found a single major ion corresponding to Gly-Pro (*m/z* 173.1), whereas free Pro appeared as two ions at *m/z* 116.1 and *m/z* 118.1, demonstrating incorporation of ^{18}O in the peptidolytic N-terminal leaving group (i.e., Pro) (Fig. S2). Together, these mass spectrometric data unambiguously demonstrate that Pro-Gly-Pro is cleaved by LTA4H according to an aminopeptidase mechanism.

Mechanism for LTA4H-Catalyzed Pro-Gly-Pro Hydrolysis and Identification of the Catalytic Water. With this information at hand, we analyzed the crystal structure of LTA4H in complex with OPB-Pro to detail the aminopeptidase mechanism. The substrate analog aligns in the active site cavity anchored by the side chains of Glu271 and Arg563 at its N terminus and C terminus, respectively, in two slightly

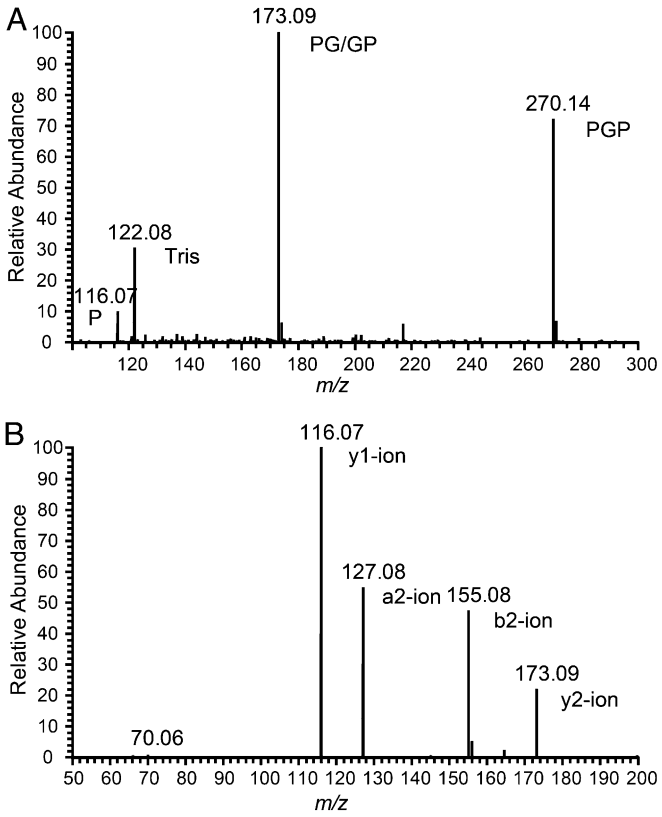

Fig. 3. MS analysis of products generated from Pro-Gly-Pro by LTA4H. (*A*) MS analysis of Pro-Gly-Pro hydrolysis products [0.01 μg/μL LTA4H and 200 μM Pro-Gly-Pro (PGP), filtered]. The primary spectrum contains a major ion at *m/z* 173.1, corresponding to both Pro-Gly (PG) and Gly-Pro (GP), as well as the peaks for Pro (P) and remaining PGP. (*B*) Collision-induced dissociation mode (CID) MS/MS spectra of the product peak at *m/z* 173.1 leads to a fragmentation spectrum containing a peak at *m/z* 116.2, corresponding to the characteristic y1-ion of the dipeptide GP. The spectrum also contains the a2-, b2-, and y2-ions.

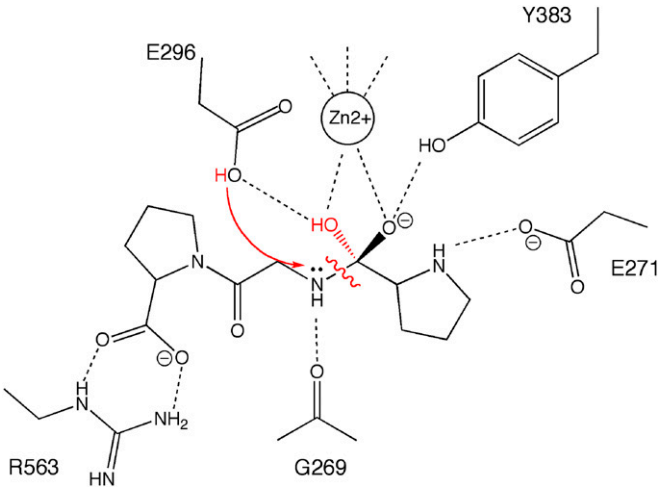

Fig. 4. Mechanism for enzymatic hydrolysis of Pro-Gly-Pro by LTA4H. The figure depicts a transition state in a general base mechanism for N-terminal cleavage of Pro-Gly-Pro, involving Glu296, Tyr383, Zn^{2+}, and a catalytic water (in red). Due to space limitations, the three zinc-binding ligands His295, His299, and Glu318 are only indicated with lines.

different conformations denoted A and B (Fig. 2 and Fig. S3). Based on mechanistic considerations and distances between OPB-Pro and catalytic elements at the active site, conformation A likely reflects a transition state, whereas conformation B appears to be the result of substitution of the substrate's glycyl nitrogen for a carbon atom in OPB-Pro (Fig. S3).

In conformation A, the N-terminal nitrogen of OPB-Pro interacts with the $O^{\varepsilon 2}$ atom of Glu271 through hydrogen bond with distance of 2.80 Å, whereas the C terminus is hydrogen-bonded to the guanidinium group of Arg563 with distances of 2.86 and 3.05 Å. After several cycles of restrained refinement of the structure model with ligands, two additional $mF_o - DF_c$ density peaks greater than 3.5 σ above the mean were found close to the zinc-binding site. These peaks were modeled as two half-occupied catalytic waters, denoted H_2O-1 and H_2O-2. Both waters were stabilized by interaction with Zn^{2+} at a distance of 2.75 Å for H_2O-1 and 1.85 Å for H_2O-2 (Fig. 2 and Fig. S3).

In conformation A, the carbonyl oxygen of the N terminus of OPB-Pro is coordinated with Zn^{2+} (distance of 1.84 Å) and hydrogen-bonded with the hydroxyl group of Tyr383 (2.80 Å). The catalytic water H_2O-1 is at a distance of 2.69 Å from $O^{\varepsilon 2}$ of the catalytic base, Glu296. During modeling of an alternative conformation A for OPB-Pro and H_2O-1, we noticed that the distance of 1.47 Å between the water oxygen and the carbon atom of the carbonyl group is too short to allow the presence of two molecules simultaneously. Therefore, we believe that this complex represents a trapped tetrahedral transition state, including a catalytic water, that cannot be further processed owing to the lack of the substrate's glycyl nitrogen in OPB-Pro (Fig. 2). This complex structure agrees well with previous conclusions regarding the aminopeptidase mechanism of LTA4H and predicts that Pro-Gly-Pro is cleaved according to a general base mechanism (4). The catalytic zinc is complexed by His295, His299, Glu318, and an activated water molecule, which is observed as H_2O-1 in the OPB-Pro/LTA4H complex structure (Fig. 4). The N terminus is anchored to Glu271, whereas the C terminus is bound by Arg563. The catalytic water is displaced from the zinc atom by the carbonyl oxygen of the tripeptide and polarized by Glu296 to promote an attack on the carbonyl carbon of the scissile peptide bond. The oxyanion intermediate is stabilized by Tyr383 and the zinc. In the final reaction step, Glu296 shuffles a proton from the hydrolytic water to the leaving group. Details

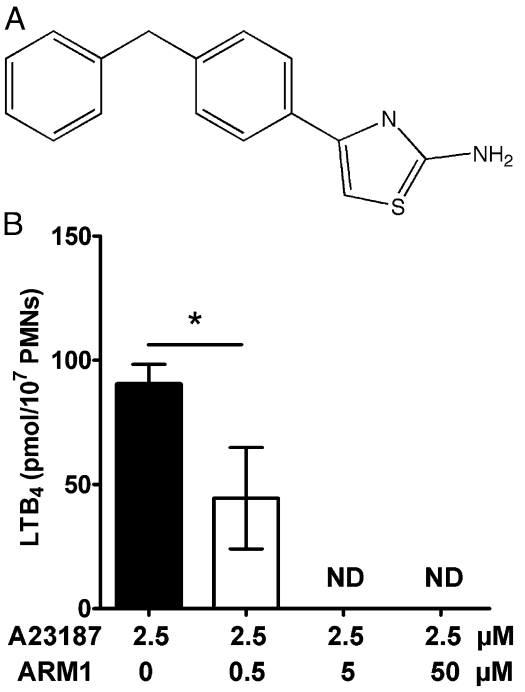

Fig. 5. ARM1 inhibits LTB_4 synthesis in human PMNs. (*A*) Chemical structure of ARM1. (*B*) Isolated human PMNs (10×10^6 per milliliter) were treated with 0, 0.5, 5, and 50 μM ARM1 prior to stimulation with ionophore A23187 (2.5 μM) for 5 min at 37 °C. Generation of LTB_4 was assessed by reverse-phase HPLC. ND, not detected. $*P < 0.05$.

of the B conformation of the OPB-Pro/LTA4H complex structure are provided in *Supporting Information* and Fig. S3.

Identification of a Selective Epoxide Hydrolase Inhibitor. Because the binding of Pro-Gly-Pro at the active site seemed to leave space within the narrow hydrophobic cavity, we began searching for molecules that could potentially inhibit LTA_4 binding without interfering with Pro-Gly-Pro hydrolysis. As a starting point, we used the structure of LTA4H in complex with the inhibitor SC-57461A (*N*-[3-(4-benzylphenoxy)propyl]-*N*-methyl-β-alanine) [Protein Data Bank (PDB) ID code 3U9W], a prototype of a potent LTA4H inhibitor (Fig. S4). Here, the ultimate phenyl ring of the bicyclical portion of the inhibitor is located at the end of the hydrophobic pocket near three structural water molecules, providing a chemical environment for binding of cyclical structures with hydrophilic substituents (Fig. S4). Through in silico design and database searches, we arrived at a set of candidate inhibitors that were tested for their ability to block conversion of LTA_4 into LTB_4 by LTA4H (Table S2). One of these substances [i.e., 4-(4-benzylphenyl)thiazol-2-amine (ARM1)] was found to inhibit the epoxide hydrolase activity of purified LTA4H with a K_i of 2.3 μM. Furthermore, ARM1 efficiently inhibited LTB_4 synthesis in isolated human polymorphonuclear neutrophils (PMNs) with an IC_{50} of about 0.5 μM and complete inhibition at 5 μM. Thus, in three separate experiments with cells from different donors, human PMNs stimulated with 2.5 μM A23187 generated 90.5 ± 7.9 pmol of LTB_4 per 10^7 PMNs. After pretreatment with 0.5 μM ARM1, LTB_4 biosynthesis was reduced to 44.5 ± 20.4 pmol per 10^7 PMNs (Fig. 5). We then tested ARM1 in our standard aminopeptidase assay with Ala-*p*-nitroanilide as a substrate and found that ARM1 stimulated the specific activity ~2.5-fold (at 4 μM of ARM1), and this effect was even more pronounced against Val-*p*-nitroanilide, the specific hydrolysis of which was stimulated ~25-fold (Fig. 6). Most importantly, we tested ARM1 as an inhibitor of LTA4H-catalyzed hydrolysis of Pro-Gly-Pro and could not observe any inhibition at concentrations between 1 and 100 μM in the ninhydrin assay (Fig. 6). At concentrations of ARM1 >200 μM, a dose-dependent, albeit weak, inhibition (~35% at 1 mM) was observed. Because the ninhydrin assay is colorimetric and measures free Pro, we also used MS to test whether Pro-Gly-Pro is cleaved by LTA4H in the presence of 100 μM ARM1 and could verify robust hydrolysis of the tripeptide into Gly-Pro (Fig. S5). We conclude that ARM1 inhibits the epoxide hydrolase activity of LTA4H without significantly affecting the enzyme's ability to cleave Pro-Gly-Pro.

ARM1 Occupies the Binding Site for the ω-End of LTA_4. To elucidate the molecular basis for the inhibitory profile of ARM1, we solved the crystal structure of LTA4H in complex with ARM1 at 1.65 Å. ARM1 binds at the end of the L-shaped hydrophobic cavity believed to accommodate the ω-end of LTA_4 (Fig. 1). Here, ARM1 was modeled in two possible conformations of the thiazol-2-amine ring with equal occupancy (Fig. 7). The amino group can be anchored to the main chain of LTA4H through two hydrogen bonds to the carbonyl oxygens of Phe362 (2.67 Å) and Lys364 (2.75 Å), and by van der Waals contacts between the ring sulfur and carbonyl oxygens of Lys364 (3.06 Å) and Leu365 (2.89 Å). Alternatively, the thiazol-2-amine ring is flipped 180° and creates hydrogen and van der Waals contacts with the carbonyl oxygens of the same amino acids. The amino group is now fixed

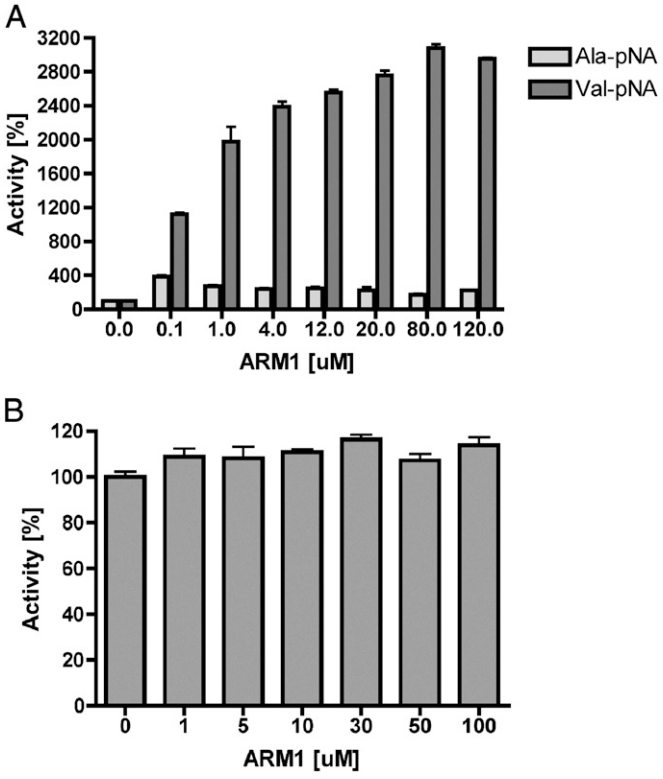

Fig. 6. Effects of ARM1 on the aminopeptidase activity of LTA4H. (*A*) Effects of different concentrations of ARM1 on peptidase activity of LTA4H against alanine-4-nitroanilide (Ala-pNA) and valine-4-nitroanilide (Val-pNA) substrates. An activity level of 100% corresponds to 479.18 nmol and 38.16 nmol of Ala-pNA and Val-pNA products (479.18 $nmol \cdot min^{-1} \cdot \mu M^{-1}$ and 38.16 $nmol \cdot min^{-1} \cdot \mu M^{-1}$) produced by human LTA4H. The bars represent mean ± SD ($n = 3$). (*B*) LTA4H was preincubated with different concentrations of ARM1, and the effects on the aminopeptidase activity against Pro-Gly-Pro were assessed by the ninhydrin assay as described in *Materials and Methods*. No inhibition was observed at the highest concentration of ARM1 tested. The activity of the enzyme without ARM1 treatment is equal to 22.28 nmol of Pro (22.28 $nmol \cdot min^{-1} \cdot \mu M^{-1}$). The bars represent mean ± SD ($n = 3$).

by hydrogen bonds with Lys364 (2.90 Å) and Leu365 (2.73 Å), whereas the thiazol sulfur is coordinated by van der Waals contacts with Phe362 (3.32 Å) and Lys364 (3.41 Å). It is interesting to note that both conformations of the thiazol-2-amine ring reach the very end of the hydrophobic cavity, even beyond the position of the ultimate phenyl ring of the bicyclical portion of SC-57461A (Fig. S4). The benzyl-phenyl moiety of the inhibitor occupies the rest of the hydrophobic cavity.

Finally, we solved the dual complex with both ARM1 and the Pro-Gly-Pro analog OPB-Pro at 1.62 Å (Fig. 8). In this structure, both OPB-Pro and ARM1 are represented in two alternative conformations identical to those found in the complex structures with each of OPB-Pro and ARM1 alone (compare Figs. 2 and 7). This structure demonstrates that Pro-Gly-Pro and the inhibitor ARM1 bind at a considerable distance from one another, at the active site of LTA4H (Fig. 8).

ARM1 Is a Lead Structure for a Novel Type of LTA4H Inhibitor. Inasmuch as LTA4H catalyzes the final and committed step in the biosynthesis of the potent chemotactic agent LTB_4, this enzyme has been an interesting target for development of anti-inflammatory drugs. Thus, several highly potent and selective inhibitors have been developed within academia as well as industry (13–16). However, none of these compounds have met the expectations and demonstrated clinical usefulness. Drug failures are common, multifactorial, and often difficult to explain. However, in the case of LTA4H inhibitors, drug failure may be related to the enzyme's aminopeptidase activity, which was believed for a long time to be physiologically unimportant. This view did not change until Snelgrove et al. (11) demonstrated that Pro-Gly-Pro, a chemotactic tripeptide derived from matrix degradation, is an endogenous substrate for LTA4H (11). For many drug discovery programs, this report arrived late; inhibition of the enzyme's aminopeptidase activity had already been used for screening of compound libraries because it is easy to monitor spectrophotometrically and is suitable for a high-throughput format. Consequently, previously developed inhibitors of LTA4H block both catalytic activities, essentially by default. Hence, to our knowledge, ARM1 is a previously unidentified inhibitor that selectively blocks the conversion of LTA_4 into LTB_4, although leaving the aminopeptidase activity intact for cleavage and inactivation of Pro-Gly-Pro, and it represents a new class of LTA4H inhibitor that holds promise for improved anti-inflammatory properties.

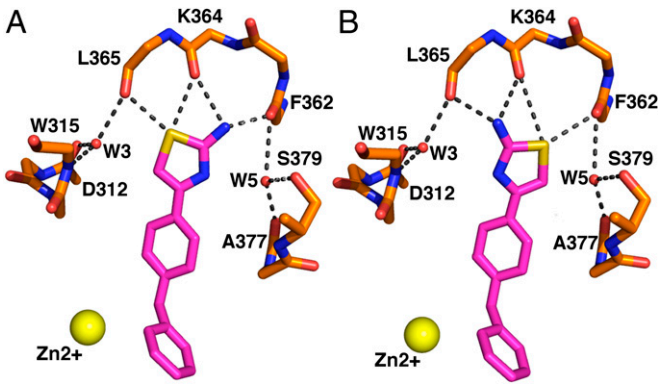

Fig. 7. Binding of ARM1 at the active site of LTA4H. ARM1 is bound in two configurations, configuration A (*A*) and configuration B (*B*), with its thiazol-2-amine at the end of the hydrophobic cavity, interacting with the backbone carbonyls of Leu365, Lys364, and Phe362 in a network that includes two structural water molecules, which are indicated as W3 and W5.

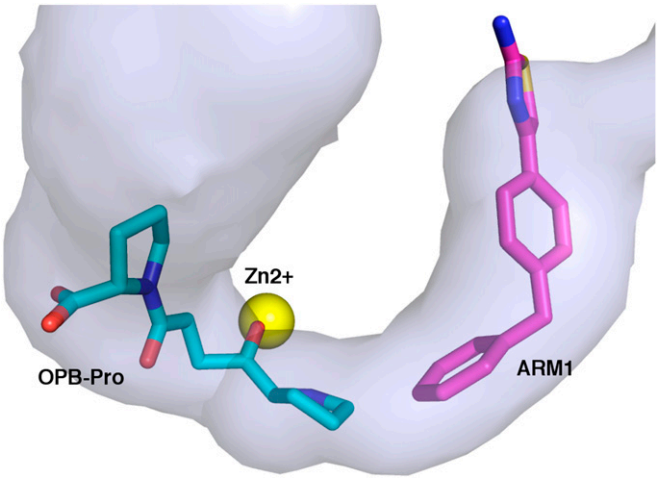

Fig. 8. Relation of OPB-Pro and ARM1 binding at the active center of LTA4H. The structure of LTA4H was solved in a double complex with both OPB-Pro and ARM1. OPB-Pro occupies the aminopeptidase active site with its prolyl carbonyl bound to the catalytic zinc, whereas ARM1 is located at the end of the hydrophobic cavity at a significant distance from the OPB-Pro.

Materials and Methods

Synthetic Pro-Gly-Pro was purchased from Cayman Chemicals. OPB-Pro was synthesized by Ramidus AB. ARM1 was obtained from Sigma. All other chemicals were purchased from standard commercial sources.

Enzyme Expression, Purification, and Activity Assays. Human recombinant LTA4H was expressed in *Escherichia coli* JM101 and purified essentially as described (17). The epoxide hydrolase activity of LTA4H was assayed by reverse-phase HPLC from incubations of enzyme with LTA_4 as described (18). For determination of K_i, LTA4H was incubated with LTA_4 (10–40 μM) and ARM1 (2–50 μM) for 1 min, and formation of LTB_4 was determined. K_i was calculated from a modified Michaelis–Menten equation for competitive inhibition in the Prism 4 program (GraphPad Software).

The aminopeptidase activity of LTA4H was assessed with Ala-*p*-Na (alanine-4-nitroanilide) and Val-*p*-Na (valine-4-nitroanilide) as substrates (18). For determination of Pro-Gly-Pro peptidolysis, 0.5 μg of LTA4H in 100 μL of 10 mM Tris·HCl (pH 7.8) was incubated with 800 μM Pro-Gly-Pro for 3 min at 37 °C. The reaction was stopped by addition of 150 μL of acetic acid, 150 μL of ninhydrin solution (25 mg/mL) was added, and the samples were allowed to stand on a heat block at 100 °C for 45 min. Toluene (350 μL) was added, and the upper phase was transferred to a 96-well plate (Greiner Bio-One). All incubations were carried out in triplicate, and absorbance was measured at 495 nm. Additional details and descriptions are provided in *SI Materials and Methods*.

Isolation and Incubation of PMNs. Human PMNs were isolated from freshly prepared buffy coats (Karolinska Hospital blood bank), and the effect of ARM1 on LTB_4 synthesis was assessed as described in *SI Materials and Methods*.

Electrospray Ionization-MS/MS Analysis. The samples were diluted 1:2 in 25% (vol/vol) acetonitrile and 0.2% formic acid, and loaded onto a 96-well microtiter plate (Abgene PCR plate; Thermo Scientific) previously rinsed with 100% (vol/vol) ethanol. The plate was placed into the Triversa Nanomate chip-based electrospray device (Advion Biosciences) operated by Chipsoft version 8.3.1.1018 (Thermo Scientific).

Five microliters of sample was picked up and directly injected into an LTQ-Orbitrap Velos mass spectrometer (Thermo Scientific). Ionization voltage was 1.45 kV, gas pressure was 0.5 psi, and capillary temperature was 250 °C. The samples' spray characteristics were stable (greater than 10 min), with an ion current between 10 and 90 nA. Survey scans were acquired in the Orbitrap with an *m/z* range of 350–2,000 and a resolution of 60,000 at *m/z* 400, and each scan comprises three coadded microscans. MS/MS spectra were obtained in collision-induced dissociation mode using a normalized collision energy of 30. The resulting fragment ions were acquired in the Orbitrap as well. Automatic gain control was used to accumulate sufficient ions for analysis with a target value of 1×10^6 and with a maximum fill time of 100 ms in full-scan mode. The mass spectra shown comprise ~20 scans. All spectra were exported from Xcalibur 2.2 (Advion Biosciences).

Crystallizations. Human LTA4H [9–11 mg/mL in 25 mM Tris·HCl buffer (pH 7.8)] was cocrystallized with 5 mM OPB-Pro, 0.2 mM ARM1, or both OPB-Pro and ARM1 for 1 h on ice. E296Q variant [10 mg/mL in 25 mM Tris·HCl buffer (pH 7.8)] was complexed with 5 mM Pro-Gly-Pro as described for LTA4H. Crystallization by liquid/liquid diffusion in capillaries (Vitrex Medical A/S) was carried out as described (10). In brief, 5 μL of protein was layered on an equal volume of precipitant solution composed of 22–30% (wt/vol) PEG 8000, 100 mM NaAc, 100 mM imidazole buffer (pH 6.5–7.0), and 5 mM $YbCl_3$. Plate-shaped crystals grew to maximum dimensions of $0.5 \times 0.3 \times 0.05$ mm within 7 d at 277 K. Prior to freezing in liquid nitrogen, the crystals were soaked in cryoprotecting solution consisting of 50% concentration of crystallizing solution and 25% (vol/vol) glycerol with the addition of the appropriate ligand in concentration used for cocrystallization.

Data Collection and Processing. Crystals of LTA4H in complex with OPB-Pro and E296Q in complex with Pro-Gly-Pro were used for X-ray diffraction analysis at beamline ID14-4 (European Synchrotron Radiation Facility, Grenoble, France) (19), which is equipped with an Q315r Area Detector Systems Corporation CCD detector. For LTA4H in complex with OPB-Pro, a single dataset (resolution of 100–1.72 Å) of 200 images was collected with an oscillation angle of 1° per image and a crystal-to-detector distance of 136 mm. Data of 195 images from a crystal of E296Q (resolution of 42.84–1.80 Å) were collected with a 0.45° oscillation angle and a crystal-to-detector distance of 268 mm. The data indexing, integration, and scaling for both proteins were done with the autoPROC software package (20).

Diffraction data for LTA4H in complex with ARM1 and with both OPB-Pro and ARM1 were collected at beamlines 14.1 and 14.2, respectively, at the Berlin Electron Storage Ring Society for Synchrotron Radiation (BESSY) II electron storage ring (21). Four hundred images of LTA4H in complex with ARM1 were recorded using a Rayonix MX-225 CCD detector. This dataset (resolution of 42.18–1.65 Å) was collected with an oscillation angle of 0.5° and a crystal-to-detector distance of 190 mm. For LTA4H in complex with OPB-Pro and ARM1 (resolution of 43.79–1.62 Å), 1,800 images with an oscillation angle of 0.1° per image and a crystal-to-detector distance of 320 mm were collected at the Dectris Pilatus 6M detector. Data for both crystals were indexed, integrated, and scaled using XDSAPP (22). The resolution cutoff for all three datasets was based on the new assessment correlation coefficient $CC_{1/2}$ criteria (23). The data collection statistics for datasets of LTA4H in complex with OPB-Pro, ARM1, and both OPB-Pro and ARM1 are summarized in Table S3.

Structure Solution, Refinement, and Validation. All structures of LTA4H were solved by the molecular replacement method using MOLREP (24) for E296Q and LTA4H in complex with OPB-Pro and both OPB-Pro and ARM1 or PHASER (25) for LTA4H in complex with ARM1. The coordinates of human LTA4H (PDB ID code 2R59) (4) were used as the search model. MOLREP and PHASER indicated one monomer in the asymmetrical unit for every structure.

All structures of LTA4H were refined in REFMAC5 (26), and manual inspection and model building were performed in Coot (27). After one cycle of rigid body and several cycles of restrained refinement, the $mF_o - DF_c$ difference map of the active sites was interpreted as zinc ion and ligands. The 3D coordinates in PDB and Crystallographic Information File format topology were generated for all ligands using the PRODRG server (28). Atomic displacement parameters of all protein, ligands, and water O atoms, as well as ions, were refined isotropically. The geometric parameters of each model were checked by MolProbity (29) and Coot validation functions. The final validation of model quality with respect to experimental data was made using REFMAC5. The coordinates and structure factors of the final models of LTA4H were deposited in the PDB (www.rcsb.org). Structure refinement, validation statistics, and accession PDB codes are presented in Table S3. The final model of E296Q in complex with Pro-Gly-Pro was not deposited due to ambiguity of the position of the ligand in the active site of enzyme. All figures with structures were made in PyMOL (30).

ACKNOWLEDGMENTS. The authors are grateful to Ms. Michaela Mårback for excellent technical assistance and advice. We thank the European Synchrotron Radiation Facility for providing access to X-ray sources, and especially local contacts at beamline ID14.4 for assistance. We thank Helmholtz-Zentrum Berlin for the allocation of synchrotron radiation and assistance at beamline 14.1 and 14.2, as well as BiostructX-783. We also thank the Protein Structure Facility at the Karolinska Institutet for providing excellent facilities for protein crystallization. This study was supported by the Swedish Research Council (Grants 621-2011-5003, 10350, and 20854 and a CERIC Linneus grant), Vinnova Foundation (CIDaT project), Stockholm County Council (Cardiovascular Program, Thematic Center Inflammation), Dr. Hans Kröner Graduiertenkolleg, and the European Union (Grant 201668). J.Z.H. is the recipient of a Distinguished Professor Award from the Karolinska Institutet.

1. Samuelsson B (1983) Leukotrienes: Mediators of immediate hypersensitivity reactions and inflammation. *Science* 220(4597):568–575.
2. Haeggström JZ (2004) Leukotriene A_4 hydrolase/aminopeptidase, the gatekeeper of chemotactic leukotriene B_4 biosynthesis. *J Biol Chem* 279(49):50639–50642.
3. Orning L, Gierse JK, Fitzpatrick FA (1994) The bifunctional enzyme leukotriene-A_4 hydrolase is an arginine aminopeptidase of high efficiency and specificity. *J Biol Chem* 269(15):11269–11273.
4. Tholander F, et al. (2008) Structure-based dissection of the active site chemistry of leukotriene A_4 hydrolase: Implications for M1 aminopeptidases and inhibitor design. *Chem Biol* 15(9):920–929.
5. Haeggström JZ, Wetterholm A, Shapiro R, Vallee BL, Samuelsson B (1990) Leukotriene A_4 hydrolase: A zinc metalloenzyme. *Biochem Biophys Res Commun* 172(3):965–970.
6. Haeggström JZ, Wetterholm A, Vallee BL, Samuelsson B (1990) Leukotriene A_4 hydrolase: An epoxide hydrolase with peptidase activity. *Biochem Biophys Res Commun* 173(1):431–437.
7. Barret AJ, Rawlings ND, Woessner JF (1998) Family M1 of membrane alanyl aminopeptidase. *Handbook of Proteolytic Enzymes*, eds Barret AJ, Rawlings ND, Woessner JF (Academic, London), pp 994–996.
8. Medina JF, et al. (1991) Leukotriene A_4 hydrolase: Determination of the three zinc-binding ligands by site-directed mutagenesis and zinc analysis. *Proc Natl Acad Sci USA* 88(17):7620–7624.
9. Wetterholm A, et al. (1992) Leukotriene A_4 hydrolase: Abrogation of the peptidase activity by mutation of glutamic acid-296. *Proc Natl Acad Sci USA* 89(19):9141–9145.
10. Thunnissen MM, Nordlund P, Haeggström JZ (2001) Crystal structure of human leukotriene A_4 hydrolase, a bifunctional enzyme in inflammation. *Nat Struct Biol* 8(2):131–135.
11. Snelgrove RJ, et al. (2010) A critical role for LTA4H in limiting chronic pulmonary neutrophilic inflammation. *Science* 330(6000):90–94.
12. Haeggström JZ, Funk CD (2011) Lipoxygenase and leukotriene pathways: Biochemistry, biology, and roles in disease. *Chem Rev* 111(10):5866–5898.
13. Yuan W, Wong C-H, Haeggström JZ, Wetterholm A, Samuelsson B (1992) Novel tight-binding inhibitors of leukotriene A_4 hydrolase. *J Am Chem Soc* 114(16):6552–6553.
14. Kachur JF, et al. (2002) Pharmacological characterization of SC-57461A (3-[methyl[3-[4-(phenylmethyl)phenoxy]propyl]amino]propanoic acid HCl), a potent and selective inhibitor of leukotriene $A(_4)$ hydrolase II: In vivo studies. *J Pharmacol Exp Ther* 300(2):583–587.
15. Rao NL, et al. (2010) Leukotriene A(4) hydrolase inhibition attenuates allergic airway inflammation and hyperresponsiveness. *Am J Respir Crit Care Med* 181(9):899–907.
16. Kirkland TA, et al. (2008) Synthesis of glutamic acid analogs as potent inhibitors of leukotriene A_4 hydrolase. *Bioorg Med Chem* 16(9):4963–4983.
17. Rudberg PC, Tholander F, Thunnissen MMGM, Haeggström JZ (2002) Leukotriene A4 hydrolase/aminopeptidase. Glutamate 271 is a catalytic residue with specific roles in two distinct enzyme mechanisms. *J Biol Chem* 277(2):1398–1404.
18. Wetterholm A, et al. (1991) Recombinant mouse leukotriene A_4 hydrolase: A zinc metalloenzyme with dual enzymatic activities. *Biochim Biophys Acta* 1080(2):96–102.
19. McCarthy AA, et al. (2009) A decade of user operation on the macromolecular crystallography MAD beamline ID14-4 at the ESRF. *J Synchrotron Radiat* 16(Pt 6):803–812.
20. Vonrhein C, et al. (2011) Data processing and analysis with the autoPROC toolbox. *Acta Crystallogr D Biol Crystallogr* 67(Pt 4):293–302.
21. Mueller U, et al. (2012) Facilities for macromolecular crystallography at the Helmholtz-Zentrum Berlin. *J Synchrotron Radiat* 19(Pt 3):442–449.
22. Krug M, Weiss MS, Heinemann U, Mueller U (2012) XDSAPP: A graphical user interface for the convenient processing of diffraction data using XDS. *J Appl Crystallogr* 45(3):568–572.
23. Karplus PA, Diederichs K (2012) Linking crystallographic model and data quality. *Science* 336(6084):1030–1033.
24. Vagin AA, Teplyakov A (1997) MOLREP: An automated program for macromolecular replacement. *J Appl Crystallogr* 30(6):1022–1025.
25. McCoy AJ, et al. (2007) Phaser crystallographic software. *J Appl Crystallogr* 40(Pt 4): 658–674.
26. Murshudov GN, Vagin AA, Dodson EJ (1997) Refinement of macromolecular structures by the maximum-likelihood method. *Acta Crystallogr D Biol Crystallogr* 53(Pt 3):240–255.
27. Emsley P, Lohkamp B, Scott WG, Cowtan K (2010) Features and development of Coot. *Acta Crystallogr D Biol Crystallogr* 66(Pt 4):486–501.
28. Schüttelkopf AW, van Aalten DM (2004) PRODRG: A tool for high-throughput crystallography of protein-ligand complexes. *Acta Crystallogr D Biol Crystallogr* 60(Pt 8): 1355–1363.
29. Chen VB, et al. (2010) MolProbity: All-atom structure validation for macromolecular crystallography. *Acta Crystallogr D Biol Crystallogr* 66(Pt 1):12–21.
30. DeLano WL (2010) The PyMOL Molecular Graphics System (Schrödinger, New York), Version 1.4.
31. Chovancova E, et al. (2012) CAVER 3.0: A tool for the analysis of transport pathways in dynamic protein structures. *PLOS Comput Biol* 8(10):e1002708.